RSC Advances

PAPER

View Article Online
View Journal | View Issue

Cite this: *RSC Adv.*, 2018, **8**, 33425

Catalytic oxidation of ethyl acetate over $LaBO_3$ (B = Co, Mn, Ni, Fe) perovskites supported silver catalysts†

Yu Qin,[a] Fangxia Shen,[a] Tianle Zhu,[a] Wei Hong[a] and Xiaolong Liu *[b]

Received 19th August 2018
Accepted 23rd September 2018

DOI: 10.1039/c8ra06933f

rsc.li/rsc-advances

A series of silver catalysts supported on lanthanum based perovskites $LaBO_3$ (B = Co, Mn, Ni, Fe) were synthesized and evaluated in the catalytic oxidation of ethyl acetate. XRD, BET, TEM/HRTEM, HAADF-STEM, XPS and H_2-TPR were conducted, and the results indicate that redox activity of the catalysts is of great importance to the oxidation reaction. Activity tests demonstrated that $Ag/LaCoO_3$ was more active than the other samples in ethyl acetate oxidation. Moreover, the CO_2 selectivity, CO_x yields and byproduct distributions for all catalysts were studied, and $Ag/LaCoO_3$ showed the best catalytic performance. Besides, $Ag/LaCoO_3$ also showed excellent catalytic activity for other OVOCs.

1. Introduction

As a common volatile organic compound (VOC) pollutant, ethyl acetate is usually used as a solvent for extracting natural flavors, cleaning textile materials and painting. Meanwhile, ethyl acetate emission may cause adverse health effects, such as headaches, nausea and even cancer.[1] Currently, various techniques have been developed to remove ethyl acetate.[2–4] Among them, catalytic oxidation is generally regarded as a highly efficient technique for reducing ethyl acetate emissions.[4–7]

Numerous catalysts have been used in the catalytic oxidation of ethyl acetate, and usually include noble metals and metal oxides. Noble metals commonly exhibit high catalytic activity in VOCs abatements.[8–10] Au catalysts have been well demonstrated in ethyl acetate oxidation, and Carabineiro *et al.* reported that Au/oxide catalysts possessed high catalytic activity for the oxidation of ethyl acetate, and pointed out that the role of gold is to enhance the reducibility of the surface of the oxide supports.[11] However, the drawbacks of high cost, instability, and sensitivity to poison have greatly limited the practical applications of noble metals in the industrial process. Recently, metal oxides have been intensively studied due to their relatively low cost and poison resistance.[12–14] Among the metal oxides, perovskite-type oxides with the general formula of ABO_3, have been widely used in air purification,[15–18] solar hydrogen production,[19] sensor[20] and diesel fuel reforming[21] due to their advantages of low cost, high thermal stability, and great catalytic performance.[22,23]

Of all the perovskite-type oxides, lanthanum (La)-based perovskites, namely $LaBO_3$, are recognized as one of the most potential catalysts with higher efficient for their B sites that can be filled with various transition metal cations.[24–26] Recently, Taran *et al.* evaluated the effects of the variation of the B sites in $LaBO_3$ (B = Cu, Fe, Mn, Co, Ni) catalysts for wet peroxide oxidation of phenol, and found that $LaCuO_3$ was the most active one, whereas $LaFeO_3$ was the most stable one.[26] Zhu *et al.* studied a series of A-site substituted $La_{0.8}M_{0.2}MnO_3$ catalysts (M = Ba, Ca, Ce, Mg and Sr) for plasma-catalytic oxidation of ethyl acetate, and found that $La_{0.8}Ce_{0.2}MnO_3$ catalyst has the highest activity, corresponding to its highest reducibility among the tested catalysts.[3] Subsequently, Zhu group investigated the plasma-catalytic oxidation of ethyl acetate with $La_{1-x}Ce_xCoO_{3+\delta}$ ($x = 0$, 0.05, 0.1, 0.3 and 0.5) catalysts.[1] The removal efficiency of ethyl acetate for the Ce-doped $LaCoO_3$ catalyst was further enhanced, because of the increased specific surface area and a reduced crystallite size compare of pure $LaCoO_3$. Giraudon *et al.* reported the oxidation of chlorobenzene over $Pd/LaBO_3$ (B = Co, Mn, Fe, Ni), and found that palladium was totally reduced in hydrogen, while the perovskite network was either unaffected or transformed with partial destruction.[27] Tang *et al.* found that $LaCoO_3$ with 3DOM structures exhibited excellent catalytic activity in soot oxidation.[28]

Meanwhile, silver-based catalysts performed well for the oxidation of various VOCs pollutants, such as ethyl acetate,[6] formaldehyde,[29] toluene,[30] methanol,[31] acetone[32] and naphthalene.[33] Jodaei *et al.* studied bimetallic Ag–M (M = Fe, Co, Mn)-ZSM-5 for its catalytic oxidation ability of ethyl acetate, and found that Ag–Fe-ZSM-5 has the highest catalytic activity.[6] Wang *et al.* reported that the Ag-doped $LaMnO_3$ perovskite oxide

[a]*School of Space and Environment, Beihang University, Beijing 100191, China*
[b]*Beijing Engineering Research Center of Process Pollution Control, National Engineering Laboratory for Hydrometallurgical Cleaner Production Technology, Institute of Process Engineering, Chinese Academy of Sciences, Beijing 100190, China. E-mail: liuxl@ipe.ac.cn*

† Electronic supplementary information (ESI) available: Specific surface areas, H_2 consumption of the samples, and byproduct distributions. See DOI: 10.1039/c8ra06933f

exhibits high activity for simultaneous removal of NO_x and diesel because of the abundant oxygen vacancy and over-stoichiometry oxygen in the perovskite lattice along with Ag^0.[34] However, few work has been done on the use of silver supported $LaBO_3$ perovskite catalysts for ethyl acetate removal. Hence, it is of great interest to investigate the silver-based $LaBO_3$ perovskite catalysts in ethyl acetate oxidation.

In this work, a series of B-site substituted Ag/$LaBO_3$ (B = Co, Mn, Ni, Fe) catalysts were synthesized and evaluated regarding their catalytic oxidation potential of ethyl acetate. The structures of Ag/$LaBO_3$ catalysts were characterized by BET, XRD, TEM/HR-TEM, HAADF-STEM, XPS and H_2-TPR, and the role of the B-site substitutes on the reaction performance was further explored. The results indicate that the reducibility of the catalysts plays a key role in the removal of ethyl acetate.

2. Experimental

2.1. Catalyst preparation

$LaBO_3$ (B = Co, Mn, Fe, Ni) perovskites were synthesized from citrate precursors as described in the literature.[35] In brief, 20 mmol of $La(NO_3)_3 \cdot 6H_2O$ and 20 mmol $B(NO_3)_x$ nitrate salts ($Co(NO_3)_2 \cdot 6H_2O$; $Mn(NO_3)_2$ (50% solution); $Ni(NO_3)_2 \cdot 6H_2O$; $Fe(NO_3)_3 \cdot 9H_2O$) as well as 40 mmol citric acid were added to 100 mL of deionized water. The mixture was stirred for 2 h and then maintained at 100 °C for 12 h. A viscous gel was obtained with the rotary evaporator, followed by drying in an oven at 100 °C for 10 h. The obtained solid was finally calcined at 700 °C for 5 h giving $LaBO_3$ perovskites. Ag/$LaBO_3$ catalysts were prepared using wet impregnation method with silver nitrate aqueous solution. After the impregnation, the samples were dried at 100 °C for 12 h and calcined at 350 °C for 3 h in air. The loading of Ag in Ag/$LaBO_3$ catalysts was 1.0 wt%.

2.2. Catalyst characterization

X-ray diffraction (XRD) of the products was carried out on a powder diffractometer (Rigaku D/Max-RA) with Cu Kα radiation (120 mA, 40 kV). The nitrogen adsorption–desorption isotherm was performed using Autosorb iQ Quantachrome system at 77 K. Transmission electron microscopy (TEM) and high-angle annular dark-field scanning TEM (HAADF-STEM) images were taken on a FEI Tecnai G^2 F20 field emission electron microscope operating at 200 kV. X-ray photoelectron spectroscopy (XPS) measurements were performed with a Thermo escalab 250Xi X-ray using Al Kα source. Hydrogen temperature programmed reduction (H_2-TPR) was detected by an AutoChemII 2920 apparatus with a flow-type reactor. Hydrogen (10 vol% in Ar) was passed through a reaction tube containing the catalyst under atmospheric pressure at 30 mL min^{-1}. The tube was heated with an electric furnace at a heating rate of 10 °C min^{-1} from 25 °C to 600 °C.

2.3. Catalytic evaluation

The $LaBO_3$ and Ag/$LaBO_3$ samples were tested in a continuous flow fixed-bed quartz microreactor (i.d. = 4 mm) from 150 °C to 350 °C with 100 mg of catalyst (60–80 mesh). The solid was placed on the quartz sieve, which was fixed in the middle of the quartz microreactor. The reaction gas consisted of 500 ppm ethyl acetate, 20% O_2, 1% H_2O (when used), and was balanced with Ar. The concentration of reaction gas was calibrated with a gas chromatography (GC 2010 Plus, Shimadzu) through a by-pass. The total flow of the reactant mixture was 100 mL min^{-1} with the weight hourly space velocity (WHSV) of 60 000 mL $(g\ h)^{-1}$.

3. Results and discussion

3.1. Catalysts characterization

Fig. 1 shows XRD patterns of the Ag/$LaBO_3$ catalysts, there appears no any new diffraction peak corresponding to Ag or Ag_2O phase mainly due to the low loading (1 wt%) of Ag and the small size of Ag nanoparticles, which has been demonstrated in Au-based catalysts.[11] All the diffraction peaks were clearly indexed which agreed with rhombohedral phase for $LaCoO_3$ (JCPDS 48-0123) and $LaNiO_3$ (JCPDS 33-711), cubic structure of $LaMnO_3$ (JCPDS 75-0440), orthorhombic phase for $LaFeO_3$ (JCPDS 15-0148), respectively. Besides, four catalysts were also characterized by BET method, and their specific surface areas (S_{BET}) were 14.5, 19.3, 12.5, and 14.0 $m^2\ g^{-1}$ for Ag/$LaCoO_3$, Ag/$LaMnO_3$, Ag/$LaNiO_3$ and Ag/$LaFeO_3$ (Table S1†), respectively, which were consistent with those of previously reported perovskite materials.[27,36]

TEM images of Ag/$LaCoO_3$ catalyst are shown in Fig. 2a with the inset of Ag particle size distribution calculated by Image-J software. The Ag particle sizes varied from 2 to 16 nm with the average value at 7.5 ± 2 nm. Moreover, the particle that corresponded to metallic Ag (111) facet with the lattice fringes of 0.24 nm was observed from the high-resolution TEM (HRTEM) (Fig. 2b). The Ag, La and Co distributions were studied by taking HAADF-STEM images and STEM-EDS mapping analysis (Fig. 2c–g). The $LaCoO_3$ nanoparticles were presented as

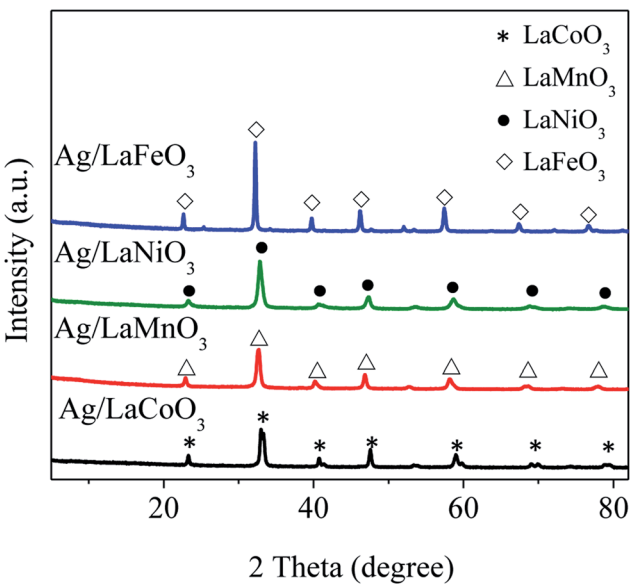

Fig. 1 XRD patterns of the Ag/$LaBO_3$ (B = Co, Mn, Ni, Fe).

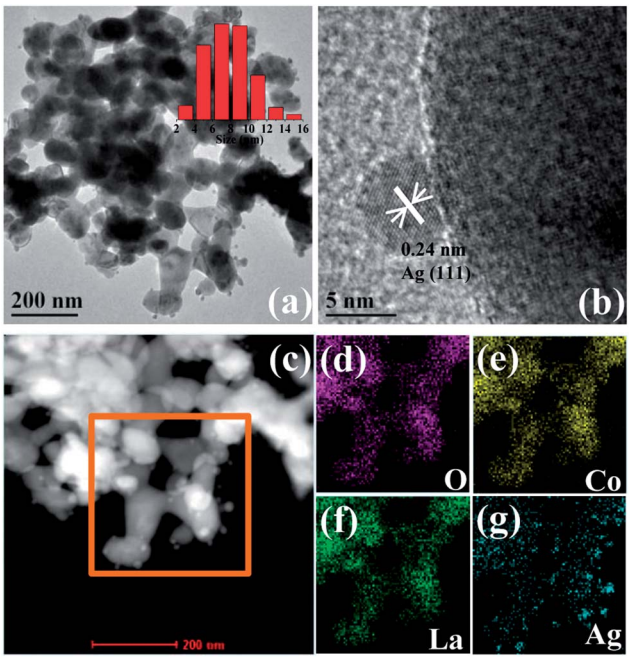

Fig. 2 TEM image (a) of the $Ag/LaCoO_3$ catalyst, with the inset histograms of Ag particle size distribution, HRTEM image (b) of Ag particles, and representative HAADF-STEM image (c) and STEM-EDS mapping images of (d) O, (e) Co, (f) La and (g) Ag for $Ag/LaCoO_3$.

bright spots in Fig. 2c. In the STEM-EDS mappings (Fig. 2d–g), the observed O (purple), Co (yellow), La (green) and Ag (blue) shows similar distributions, indicating that Ag species was well-dispersed on the $LaCoO_3$ support as metallic Ag nanoparticles.

The redox properties of $Ag/LaBO_3$ and $LaBO_3$ catalysts were investigated using H_2-TPR from 50 to 600 °C (Fig. 3). The first reduction peaks can be attributed to the reduction of surface oxygen species, which were at 319, 316, 357 and 385 °C for $LaCoO_3$, $LaMnO_3$, $LaNiO_3$ and $LaFeO_3$, respectively (Fig. 3b, d, f and h). In addition, $LaCoO_3$ (1.98 mol g^{-1}) consumes more hydrogen than $LaMnO_3$ (0.45 mol g^{-1}) (Table S2†) because of a large number of adsorption and lattice oxygen on the $LaCoO_3$ surface, suggesting that the sample with $LaCoO_3$ support was easier to be reduced than samples with other supports. For the unsupported $LaBO_3$ perovskites materials, two peaks were observed. The peak at low temperature was ascribed to the reduction of adsorbed oxygen, and the peak at high temperature was due to the reduction of lattice oxygen.[3] For $Ag/LaCoO_3$ and $LaCoO_3$, Co^{3+}/Co^{2+} and Co^{2+}/Co^0 transformation occurred in the reduction, and Co^{3+}/Co^{2+} redox play an important role in the catalytic oxidation, generating abundant mobile oxygen for the realization of the Mars van Krevelen mechanism in ethyl acetate oxidation.[11] The low hydrogen consumption by $LaFeO_3$ induced by the low adsorption and lattice oxygen implies that the stable structure of $LaFeO_3$ leads to its lowest oxidizing ability. $LaNiO_3$ has higher hydrogen consumption but lower oxidizing ability than $LaMnO_3$ which is mainly ascribed to the higher first reduction temperature of $LaNiO_3$. Particularly, distinct shifts to low temperatures of the first reduction peak were observed when $LaBO_3$ were doped with silver, indicating better oxygen mobility in silver-based catalysts compared to pure $LaBO_3$. Furthermore, $Ag/LaCoO_3$ catalyst had the highest hydrogen consumption rate of 2.04 mol g^{-1} (Table S2†), suggesting that the sample possessed the best redox among the tested catalysts.

XPS spectra were collected to obtain the element chemical states and oxygen vacancies on the catalyst surface. Fig. 4a shows the Ag 3d spectra of the $Ag/LaBO_3$ catalysts. The two

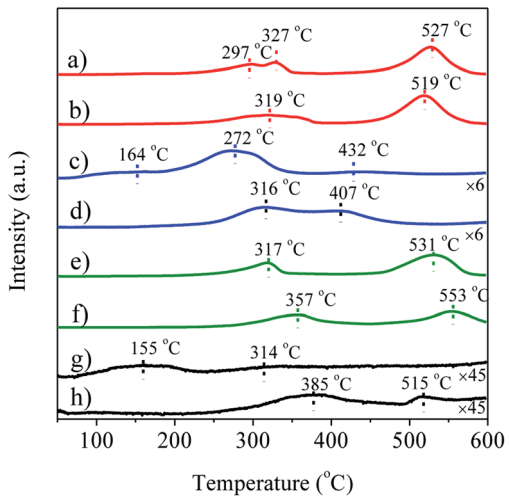

Fig. 3 H_2-TPR profiles of (a) $Ag/LaCoO_3$, (b) $LaCoO_3$; (c) $Ag/LaMnO_3$, (d) $LaMnO_3$; (e) $Ag/LaNiO_3$, (f) $LaNiO_3$; (g) $Ag/LaFeO_3$, (h) $LaFeO_3$.

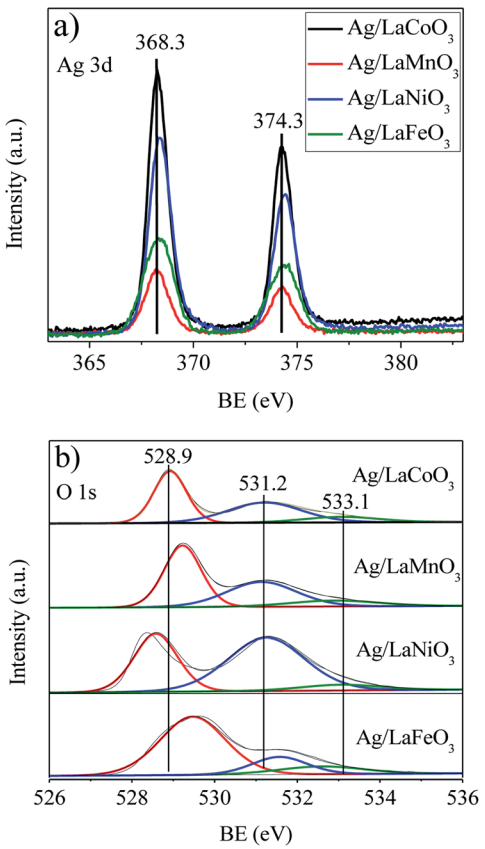

Fig. 4 XPS spectra of (a) Ag 3d and (b) O 1s for $Ag/LaBO_3$ (B = Co, Mn, Ni, Fe).

Table 1 XPS data of $Ag/LaBO_3$ (B = Co, Mn, Ni, Fe)

	Atomic composition (%)						
Sample	Ag	B	La	O	Ag/La (%)	B/La (%)	O_β/O_{total} (%)
$Ag/LaCoO_3$	2.64	13.65	18.83	64.88	0.14	0.72	41.39
$Ag/LaMnO_3$	0.74	13.26	20.57	65.43	0.04	0.64	38.12
$Ag/LaNiO_3$	2.50	5.07	18.59	73.44	0.13	0.27	57.12
$Ag/LaFeO_3$	1.60	13.9	20.05	64.45	0.08	0.69	17.70

peaks with binding energy at 368.3 and 374.3 eV correspond to the Ag $3d_{5/2}$ and Ag $3d_{3/2}$ states, respectively, which could be attributed to the Ag^0 of the metallic Ag. As listed in Table 1, $Ag/LaCoO_3$ showed the highest Ag content (2.64%), the highest ratio of Ag/La (0.14%) and B/La (0.72%) among the catalysts. The surface content of Ag on $Ag/LaNiO_3$ catalyst was 2.50%, which is lower than surface content of $Ag/LaCoO_3$ but higher than those of others, while it possessed the lowest content of B (5.07%). The Ag/La ratio on the surface of $Ag/LaMnO_3$ catalyst was the lowest, while the activity of catalytic oxidation of ethyl acetate was higher than those of $Ag/LaNiO_3$ and $Ag/LaFeO_3$. Unsupported $LaMnO_3$ contributed apparently higher catalytic activity than $LaNiO_3$ and $LaFeO_3$, due to the easy Mn^{3+}/Mn^{2+} redox, which has been demonstrated in the H_2-TPR results. Addition of Ag increased the catalytic activity of the perovskites, revealing that the Ag dispersion and B sites both play important roles in the oxidation process.

The O 1s spectra were measured to obtain the chemical states of oxygen on $Ag/LaBO_3$ catalysts (Fig. 4b). Previous reports showed that the oxygen states in perovskite-like systems were rather complex and ambiguous to interpret.[37,38] Nevertheless, the O 1s peak at the lowest binding energy may be assigned to the lattice oxygen O^{2-} and the peak at E_b = 530.8–531.5 eV assigned to oxide defects or surface oxygen ions with low coordination which is denoted as O_β, while the peak at the highest binding energy is assigned to surface carbonate or water molecules adsorbed on the surface. The relative concentration of O_β, defined as O_β/O_{total}, was calculated based on the area of the corresponding peaks (Table 1). $Ag/LaNiO_3$ with the highest O_β/O_{total} ratio showed relatively higher surface chemisorbed oxygen, although the catalytic activity was inconsistent with the amount of chemisorbed oxygen. The XPS results here suggest that the chemical states of $Ag/LaBO_3$ catalysts were affected by the B-site of the perovskite, and the catalytic activity was related to the mutual effect of content of Ag^0, ratio of Ag/La, B/La and O_β/O_{total}.

3.2. Catalytic evaluation

The $Ag/LaBO_3$ and $LaBO_3$ (B = Co, Mn, Ni, Fe) samples were evaluated in the catalytic oxidation of ethyl acetate, and the results are shown in Fig. 5. The catalysts were ranked by decreasing activity based on T_{90} as follow: $Ag/LaCoO_3$ (190 °C) > $Ag/LaMnO_3$ (203 °C) > $LaCoO_3$ (216 °C) > $Ag/LaNiO_3$ (230 °C) > $LaMnO_3$ (236 °C)> $Ag/LaFeO_3$ (267 °C) > $LaNiO_3$ (278 °C) > $LaFeO_3$ (296 °C). The result indicates that $LaCoO_3$ contributed the highest catalytic activity for the unsupported $LaBO_3$

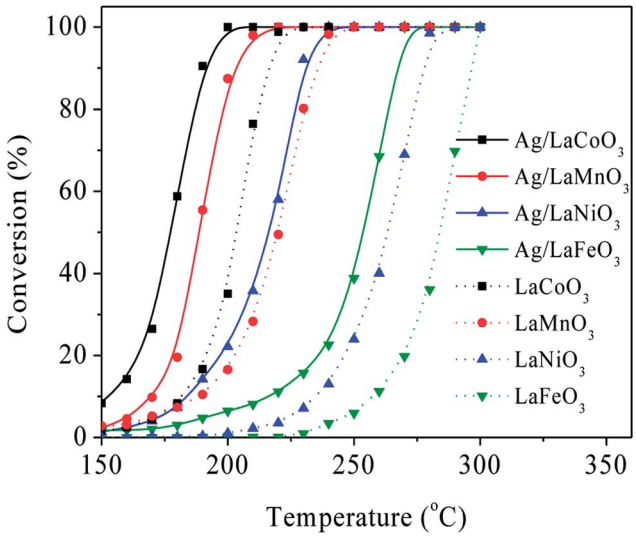

Fig. 5 Evolution of ethyl acetate conversion in function of temperature on $LaBO_3$ and $Ag/LaBO_3$ (B = Co, Mn, Ni, Fe). Ethyl acetate concentration: 500 ppm; ethyl acetate/O_2 molar ratio: 1/400; WHSV: 60 000 mL $(g\ h)^{-1}$.

perovskite materials, and addition of Ag facilitated apparently facilitated the catalytic oxidation process due to the formation Ag^0 nanoparticles and its stronger reducibility, which has been proved in the HAADF-STEM mapping images and H_2-TPR results. $Ag/LaCoO_3$ showed the highest reactivity for catalytic oxidation of ethyl acetate. According to the H_2-TPR result, $Ag/LaCoO_3$ has higher reducibility than other samples, which was crucial to the catalytic oxidation of ethyl acetate.

In order to evaluate the catalytic stability, on-stream ethyl acetate oxidation for $Ag/LaCoO_3$ was performed at 180, 190 and 200 °C, respectively. The results are summarized in Fig. 6a. When the reaction temperature was 180 °C, the ethyl acetate conversion was stabilized at 58% within 12 h, and no apparent conversion decrease was observed. With the increase of the reaction temperature, the conversion could be maintained at 90 and 99% at 190 and 200 °C, respectively, revealing that $Ag/LaCoO_3$ sample was catalytically durable.

Water vapor commonly exists in the VOCs-containing waste gases, and the anti-moisture ability is crucial to the industrial application of the catalysts. Hence, the anti-moisture experiment was evaluated for $Ag/LaBO_3$ in presence of 1% H_2O at 200 °C. As illustrated in Fig. 6b, the conversion was maintained at 99% in the first 4 h. Introduction of 1% H_2O led to the decrease of the ethyl acetate conversion from 99% to 88%, while

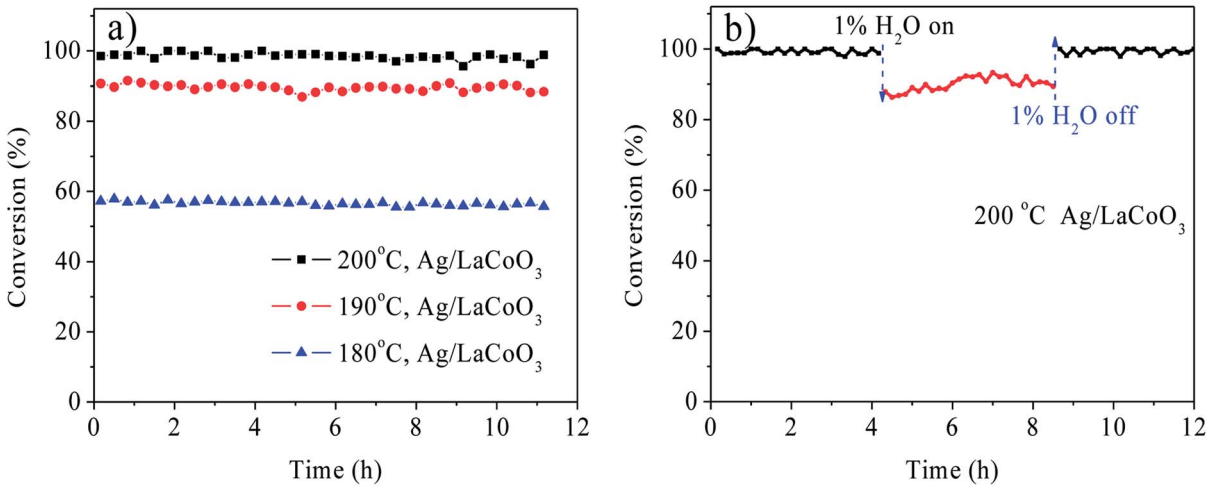

Fig. 6 The stability of ethyl acetate over $Ag/LaCoO_3$ at 180, 190 and 200 °C (a), effect of water vapor on-stream reaction over $Ag/LaCoO_3$ (b). Ethyl acetate concentration: 500 ppm; ethyl acetate/O_2 molar ratio: 1/400; WHSV: 60 000 mL (g h)$^{-1}$.

the catalytic activity was recovered when 1% H_2O was cut off. Therefore, the water exhibited an inhibitory and reversible effect in the catalytic oxidation of ethyl acetate.

To further investigate the catalytic performance, CO_2 selectivity, CO_x yields, distributions of the organic byproducts for $Ag/LaCoO_3$ and $LaCoO_3$ were studied and compared for $Ag/LaCoO_3$

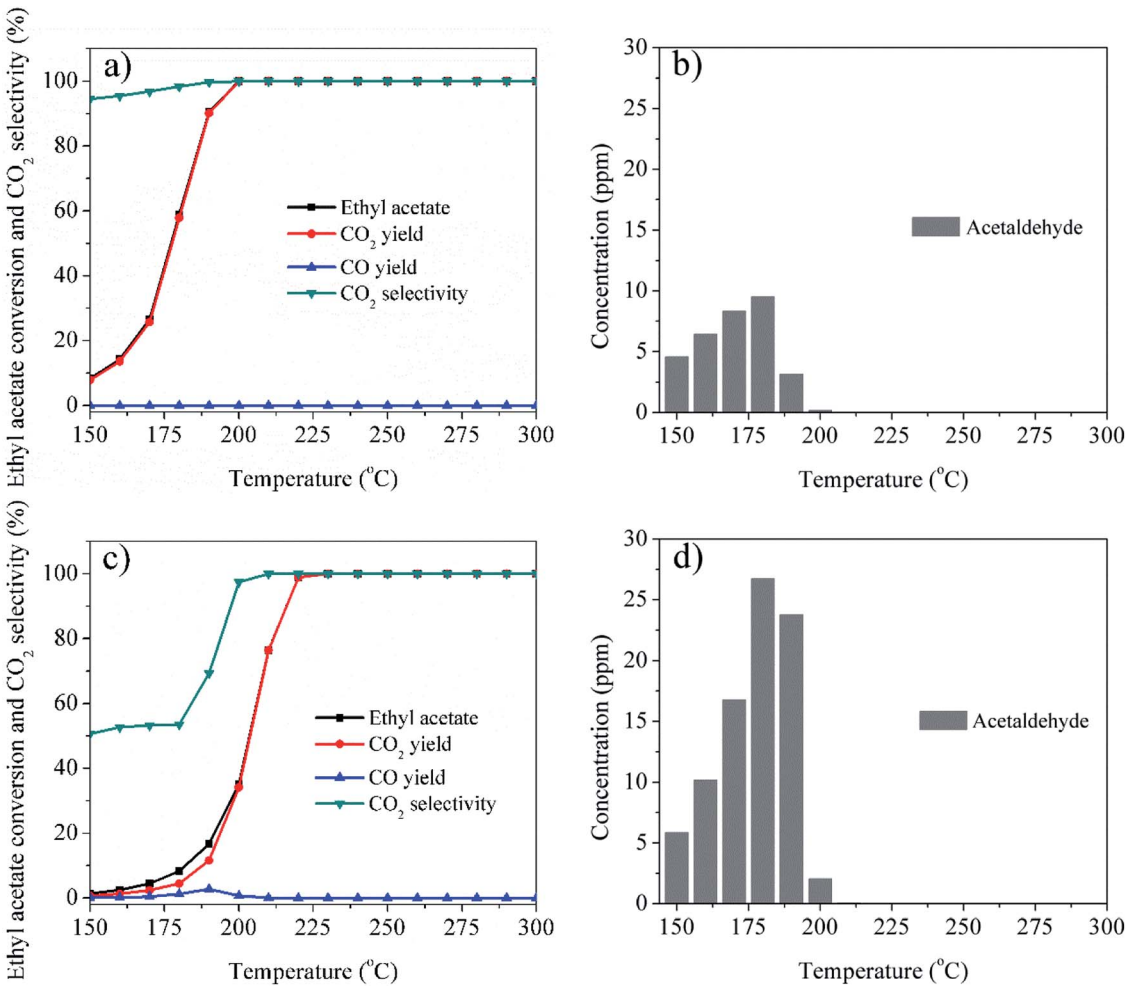

Fig. 7 Evolution of ethyl acetate conversion, CO_2 selectivity, CO_x yields, distributions of the organic byproduct in function of temperature on $Ag/LaCoO_3$ (a and b), $LaCoO_3$ (c and d). Ethyl acetate concentration: 500 ppm; ethyl acetate/O_2 molar ratio: 1/400; WHSV: 60 000 mL (g h)$^{-1}$.

and $LaCoO_3$, and the results are shown in Fig. 7. Clearly, the addition of Ag significantly promoted the removal of ethyl acetate and the selectivity of CO_2, and the CO_2 yield are almost equal to the ethyl acetate conversions in the whole experimental temperature for $Ag/LaCoO_3$. Notably, no CO was observed in the catalytic oxidation over $Ag/LaCoO_3$, whereas the CO yield reached 2.8% at 190 °C for $LaCoO_3$. As shown in Fig. 7b and d, acetaldehyde was observed and detected as the main byproduct due to the partial oxidation of ethyl acetate. It is known that ethyl acetate oxidation is a stepwise process with a preliminary hydrolysis to ethanol and acetic acid.[1] Further oxidation of ethanol contributed acetaldehyde, which was easily released from the catalyst surface as byproduct. It has been reported that surface acidity facilitates the adsorption of VOCs,[39] whereas perovskites materials commonly exhibits weak surface acidity, which might be a reason for the byproduct releasing.[40] The maximum concentration of acetaldehyde reached 9.5 and 26.7 ppm at 180 °C for $Ag/LaCoO_3$ and $LaCoO_3$, respectively, suggesting that $Ag/LaCoO_3$ possesses the advantages of higher CO_2 selectivity and less byproduct due to Ag addition. For comparison, the CO_2 selectivity, CO_x yields, distributions of the organic byproduct for $Ag/LaMnO_3$ and $LaMnO_3$ (Fig. S1†), $Ag/LaNiO_3$ and $LaNiO_3$ (Fig. S2†), $Ag/LaFeO_3$ and $LaFeO_3$ (Fig. S3†) have been collected and summarized in ESI.† It can be seen that $Ag/LaCoO_3$ and $LaCoO_3$ generates far less byproducts than other perovskite materials at similar conversions, demonstrating their high catalytic activities, which were well-correlated with their physicochemical properties. Addition of Ag commonly decreased the byproduct generations. The maximum concentrations of acetaldehyde were 22.1, 28.1, and 30.8 ppm for $Ag/LaMnO_3$, $Ag/LaNiO_3$, and $Ag/LaFeO_3$, respectively, apparently higher than that of $Ag/LaCoO_3$.

Other kinds of OVOCs such as the ethers, alcohols, and ketones, commonly exist in the industrial waste gases. Hence, the most efficient catalyst $Ag/LaCoO_3$ was also employed in the catalytic oxidation of diethyl ether, ethanol and acetone to test its oxidation ability to various OVOCs abatements. As summarized in Fig. 8, the T_{90} of ethanol, ethyl acetate, acetone, and diethyl ether were 159 °C, 190 °C, 209 °C, and 239 °C, respectively, demonstrating that $Ag/LaCoO_3$ exhibits outstanding applicability to various OVOCs purifications.

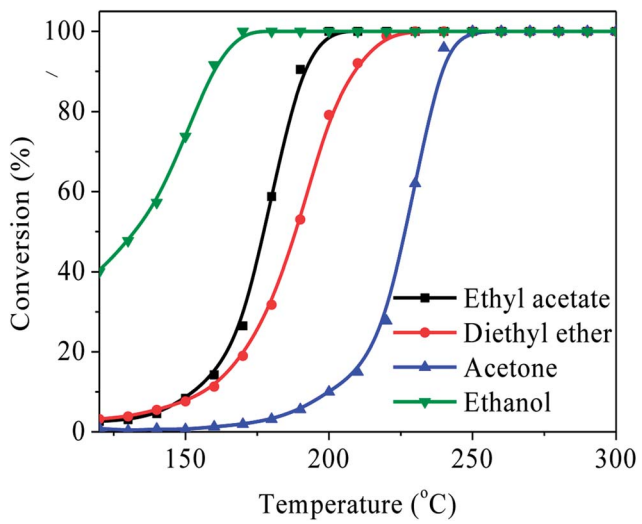

Fig. 8 Various OVOCs (ethyl acetate, diethyl ether, acetone, ethanol) conversions as a function of reaction temperature over $Ag/LaCoO_3$ under the conditions of OVOC concentration: 500 ppm; $OVOC/O_2$ molar ratio: 1/400; WHSV: 60 000 mL (g h)$^{-1}$.

4. Conclusions

In summary, $LaBO_3$ and $Ag/LaBO_3$ (B= Co, Mn, Ni, Fe) were investigated for catalytic oxidation of ethyl acetate. The synergistic effect of silver and $LaBO_3$ is a significant factor which influences the activity of catalytic oxidation. Silver supported $LaBO_3$ samples were more active than perovskite alone for ethyl acetate oxidation. Among the catalysts, $Ag/LaCoO_3$ exhibited the highest conversion rate of ethyl acetate and possessed the highest redox activity, which indicates that the reducibility of the catalysts plays a significant role in the catalytic oxidation process. $Ag/LaCoO_3$ shows excellent catalytic stability and anti-moisture performance. $Ag/LaCoO_3$ shows higher CO_2 selectivity and produces less byproduct than other samples. Moreover, $Ag/LaCoO_3$ also shows outstanding applicability for other OVOCs.

Conflicts of interest

There are no conflicts to declare.

Acknowledgements

This work was supported by National Key R&D Program of China (Grant no. 2016YFC0207103) and Natural Science Foundation of China (Grant no. 21607154).

Notes and references

1 X. Zhu, S. Zhang, Y. Yang, C. Zheng, J. Zhou, X. Gao and X. Tu, *Appl. Catal., B*, 2017, **213**, 97–105.
2 C. H. Wu and C. W. Lin, *J. Taiwan Inst. Chem. Eng.*, 2016, **68**, 332–337.
3 X. Zhu, X. Tu, M. Chen, Y. Yang, C. Zheng, J. Zhou and X. Gao, *Catal. Commun.*, 2017, **92**, 35–39.
4 Y. Zhou, H. Zhang and Y. Yan, *J. Taiwan Inst. Chem. Eng.*, 2018, **84**, 162–172.
5 G. N. Pirogova, R. I. Korosteleva, N. M. Panich, T. A. Lagutina and Y. V. Voronin, *Russ. Chem. Bull.*, 1994, **43**, 551–554.
6 A. Jodaei, D. Salari, A. Niaei, M. Khatamian and N. Çaylak, *Environ. Technol.*, 2011, **32**, 395–406.
7 A. Niaei, D. Salari, S. A. Hosseini, R. Nabavi and A. Jodaei, *Int. J. Chem. React. Eng.*, 2008, **6**, 77–90.
8 J. E. Sawyer and M. A. Abraham, *Ind. Eng. Chem. Res.*, 1994, **33**, 2084–2089.
9 S. Akram, L. Chen, Q. Wang, X. Zhang, N. Han, G. Shen, Z. Wang and G. Ge, *Catal. Lett.*, 2017, **147**, 1–13.
10 V. P. Santos, S. A. C. Carabineiro, P. B. Tavares, M. F. R. Pereira, J. J. M. Órfão and J. L. Figueiredo, *Appl. Catal., B*, 2010, **99**, 198–205.

11 S. A. C. Carabineiro, X. Chen, O. Martynyuk, N. Bogdanchikova, M. Avalos-Borja, A. Pestryakov, P. B. Tavares, J. J. M. Órfão, M. F. R. Pereira and J. L. Figueiredo, *Catal. Today*, 2015, **244**, 103–114.
12 B. Aellach, A. Ezzamarty, J. Leglise, C. Lamonier and J. F. Lamonier, *Catal. Lett.*, 2010, **135**, 197–206.
13 X. Chen, S. A. C. Carabineiro, S. S. T. Bastos, P. B. Tavares, J. J. M. Órfão, M. F. R. Pereira and J. L. Figueiredo, *J. Environ. Chem. Eng.*, 2013, **1**, 795–804.
14 Z. Zhang, Z. Jiang and W. Shangguan, *Catal. Today*, 2016, **264**, 270–278.
15 B. Białobok, J. Trawczyński, W. Miśta and M. Zawadzki, *Appl. Catal., B*, 2007, **72**, 395–403.
16 M. M. E. Geurts, J. Talsma, J. R. B. J. Brouwers and J. J. De Gier, *Catal. Today*, 2011, **176**, 449–452.
17 M. Alifanti, M. Florea and V. Pârvulescu, *Appl. Catal., B*, 2007, **70**, 400–405.
18 P. R. Zonouz, A. Niaei and A. Tarjomannejad, *J. Taiwan Inst. Chem. Eng.*, 2016, **65**, 276–285.
19 S. Hu and M. Zhu, *Chempluschem*, 2016, **81**, 1202–1208.
20 P. K. Sekhar, R. Mukundan, E. Brosha and F. Garzon, *Sens. Actuators, B*, 2013, **183**, 20–24.
21 J. A. Villoria, M. C. Alvarez-Galvan, S. M. Al-Zahrani, P. Palmisano, S. Specchia, V. Specchia, J. L. G. Fierro and R. M. Navarro, *Appl. Catal., B*, 2011, **105**, 276–288.
22 M. A. Peña and J. L. Fierro, *Chem. Rev.*, 2001, **32**, 1981–2017.
23 Q. Yang, G. Liu and Y. Liu, *Ind. Eng. Chem. Res.*, 2017, **57**, 1–17.
24 M. Ghasdi and H. Alamdari, *Sens. Actuators, B*, 2010, **148**, 478–485.
25 J. Gallego, F. Mondragon and C. Batiot-Dupeyrat, *Appl. Catal., A*, 2013, **450**, 73–79.
26 O. P. Taran, A. B. Ayusheev, O. L. Ogorodnikova, I. P. Prosvirin, L. A. Isupova and V. N. Parmon, *Appl. Catal., B*, 2016, **180**, 86–93.
27 J.-M. Giraudon, A. Elhachimi and G. Leclercq, *Appl. Catal., B*, 2008, **84**, 251–261.
28 L. Tang, Z. Zhao, Y. Wei, J. Liu, Y. Peng and K. Li, *Catal. Today*, 2017, **297**, 131–142.
29 M. Lei, D. Wang, J. Li, B. Bai, L. Fu and Y. Li, *Appl. Catal., B*, 2014, **148–149**, 36–43.
30 H. Yang, J. Deng, Y. Liu, S. Xie, Z. Wu and H. Dai, *J. Mol. Catal. A: Chem.*, 2016, **414**, 9–18.
31 N. Shimoda, S. Umehara, M. Kasahara, T. Hongo, A. Yamazaki and S. Satokawa, *Appl. Catal., A*, 2015, **507**, 56–64.
32 S. Scirè, P. M. Riccobene and C. Crisafulli, *Appl. Catal., B*, 2010, **101**, 109–117.
33 M. Liu, X. Wu, S. Liu, Y. Gao, Z. Chen, Y. Ma, R. Ran and D. Weng, *Appl. Catal., B*, 2017, **219**, 231–240.
34 K. Wang, L. Qian, L. Zhang, H. Liu and Z. Yan, *Catal. Today*, 2010, **158**, 423–426.
35 J. M. Giraudon, A. Elhachimi, F. Wyrwalski, S. Siffert, A. Aboukaïs, J. F. Lamonier and G. Leclercq, *Appl. Catal., B*, 2007, **75**, 157–166.
36 K. Y. A. Lin, Y. C. Chen and Y. F. Lin, *Chem. Eng. Sci.*, 2017, **160**, 96–105.
37 J. L. Hueso, A. Caballero, M. Ocaña and A. R. González-Elipe, *J. Catal.*, 2008, **257**, 334–344.
38 J. N. Kuhn and U. S. Ozkan, *J. Catal.*, 2008, **253**, 200–211.
39 F. Bertinchamps, C. Grégoire and E. M. Gaigneaux, *Appl. Catal., B*, 2006, **66**, 1–9.
40 G. Pecchi, P. Reyes, R. Zamora, L. E. Cadús and J. L. G. Fierro, *J. Solid State Chem.*, 2008, **181**, 905–912.